RSC Advances

ROYAL SOCIETY OF CHEMISTRY

www.rsc.org/advances

1   **Molecular Mechanism of Action of K(D)PT as an IL-1RI**

2   **Antagonist for the Treatment of Rhinitis**

3   Chanjuan Li[1], Hu Ge[1], Lujia Cui[2], Yali Li[1], Bao Cheng[1], Guodong Zhang[1], Ziying

4   Zhang[1], Hao Qi[1], Yan Ruan[2], Qiong Gu[1*], and Jun Xu[1*]

5

6   *1 School of Pharmaceutical Sciences & Institute of Human Virology, Sun*

7   *Yat-Sen University, 132 East Circle Road at University City, Guangzhou,*

8   *510006, China. 2 No. 1 Affiliated Hospital, Guangzhou University of Chinese*

9   *Medicine, Guangzhou, 510006, China.*

10

11   **Abstract**

12   ***Background:*** Interleukin-1 receptor type I (IL-1RI) is critical for both innate

13   immunity and inflammation. IL-1RI stimulates thymocyte proliferation and the

14   release of several interleukin cytokines. These properties have increased interest in

15   targeting IL-1RI for the treatment of inflammatory diseases. Here, an IL-1RI

16   antagonist, K(D)PT (Lys-D-Pro-Thr), was tested in an allergic rhinitis model. The

17   mechanism of action was then investigated.

18

19   ***Methods:*** HEK293/IL-1RI cells and an allergic rhinitis animal model were treated

20   with K(D)PT to evaluate its therapeutic effects. Fifty nanosecond (ns) molecular

21   dynamic (MD) simulations were performed on the K(D)PT/IL-1RI complex,

22   unliganded IL-1RI, and the IL-1β/IL-1RI complex to explore the mechanism of action

23   of K(D)PT.

24

25   ***Results:*** K(D)PT down-regulated the IL-1RI-mediated induction of IL-2 and IL-4

26   mRNA expression by IL-1β in HEK293/IL-1RI cells. In addition, nose itching was

27   alleviated in mice treated with K(D)PT. Serum levels of IL-2 and IL-4 as well as

28   eosinophil infiltration were also reduced. The data suggested that IL-1RI was highly

29   expressed in the nasal mucosa of mice with allergic rhinitis. MD simulations revealed

30   the following: (1) IL-1RI remains in the open conformation in the IL-1RI/IL-1β

31   complex; (2) in unliganded IL-1RI, domains I and III randomly moved closer and

32   apart without any significant energetic changes; (3) K(D)PT locks the C- and N-

33   terminals of IL-1RI by forming hydrogen bonds with both terminals to adopt a closed

34   conformation and consequently minimizes the system energy.

35

36   ***Conclusions:*** IL-1RI antagonist K(D)PT effectively treated allergic rhinitis. The

37   molecular mechanism of action indicated that K(D)PT connects the C- and N-

38   terminals of IL-1RI via hydrogen bond formation to establish a stable conformation

39   and consequently minimize the system energy of IL-1RI.

40

41   **1.   Introduction**

42   Allergic rhinitis, which causes sneezing, rhinorrhea, and nasal obstruction, is an

43   immune system disorder mediated by IgE in response to exposure to allergens, such

44   as house dust or pollen. Allergic rhinitis results in complications such as sleep

45   disorders, sinus diseases, and asthma flares. Histologically, allergic rhinitis is

46   characterized by a significant increase in eosinophils in the respiratory mucosa and

47   epithelium. Disrupting the balance between TH1 and TH2 cells results in an increased

48   number of eosinophils[1, 2]. The TH2 cytokine IL-4 induces IgE production,

49   eosinophilia, and the release of eosinophil cationic protein[1, 3, 4]. H1 anti-histamine

50   agents remain the predominant treatments for allergic rhinitis, for example, cetirizine.

51   The acceptability of these therapeutics is limited by their failure as anti-inflammatory

52   agents[5]. Other treatments, such as neural pathway inhibitors and allergen-specific

53   immunotherapies, either possess severe side effects or are longer, complicated

54   therapeutic options[6-10]. Targeting a single cytokine, such as tumor necrosis factor-α

55   (TNF-α), is an effective strategy for treating inflammatory diseases (for example,

56   rheumatoid arthritis)[11, 12], increasing interest in therapies targeting cytokines and

57   chemokines. A challenge in this therapeutic approach is the selection of the

58   appropriate cytokine or chemokine targets because allergic rhinitis can express many

59   cytokines with overlapping functions[13]. Many cytokines are induced when IL-1RI is

60   activated because IL-1RI plays a key role in both innate immunity and inflammation.

61   IL-1RI stimulates thymocyte proliferation, accessory growth factor activity for certain

62   T helper cells, and the release of several interleukin cytokines[14-16]. Therefore, IL-1RI

63   is closely associated with allergic diseases, including allergic rhinitis, asthma, and

64   skin inflammation[17]. Drugs targeting IL-1 or IL-1R are currently clinically available

65   (for example, Anakinra, IL-1 trap, and Pralnacasan). Anakinra is an IL-1 inhibitor

66   used to treat inflammatory diseases[18, 19]. However, the short half-life of Anakinra

67   limits its acceptability[20].

68   　IL-1RI consists of three extracellular immunoglobulin domains that host an innate

69   agonist (IL-1β), undergo a conformational change, and recruit an IL-1RI accessory

70   protein (IL-1RAcP) to form an active heterodimer[21-23]. The tri-peptide K(D)PT is

71   derived from α-MSH (residues 11-13) by replacing Pro12 with D-Pro, and Val13 with

72   Thr[24-28]. K(D)PT is also associated with the IL-1β (residues 193-195)[29] and exerts

73   anti-inflammatory effects through IL-1RI[24-28]. Dominik Bettenworth and co-workers

74   demonstrated that K(D)PT is effective against intestinal inflammation in a mouse

75   model of chronic enterocolitis[30].

76   　We hypothesized that IL-1RI antagonist K(D)PT may exhibit anti-rhinitis activity.

77   To prove this hypothesis, we examined the ability of K(D)PT to antagonize IL-1RI

78   using HEK293/IL-1RI cells and tested the functional activity of K(D)PT in an animal

79   model. MD simulations were performed to determine the binding mode for the

80   K(D)PT/IL-1RI complex. There are two IL-1RI co-crystal structures, IL-1RI with the

81   agonist IL-1β (Complex A) and IL-1RI with an antagonist[31] (Complex B). Complex A

82   is structurally open, and Complex B is structurally closed. 50 ns MD simulations were

83   performed on unliganded IL-1RI, the IL-1RI/IL-1β complex, and the IL-1RI/K(D)PT

84   complex to elucidate the different binding mechanisms of Complexes A and B. These

85   differences may enable the rational design of IL-1RI antagonists.

86

87   **2.   Results**

88   2.1 K(D)PT down-regulates the IL-1RI mediated expression of IL-2 and IL-4

89   T lymphocytes play a pivotal role in the process of airway hyper-responsiveness,

90   which is the main cause of allergic rhinitis and asthma[32]. The role of T lymphocytes

91   involves the production of various inflammatory cytokines and consequently affects

92   downstream signaling[33]. Among these cytokines, IL-2 and IL-4 are considered

93   responsible for T cell resistance in airway inflammation[34]. Therefore, to elucidate the

94   regulatory effects of K(D)PT on the expression of IL-2 and IL-4, we selected the

95   HEK293/IL-1RI cell line[15], which overexpresses IL-1RI, to perform RT-PCR assays.

96   The mRNA expressions of IL-2 and IL-4 were significantly up-regulated in cells

97   stimulated with 10 ng/ml IL-1β (Figure 1). K(D)PT significantly down-regulated the

98   mRNA expressions of IL-2 and IL-4 in a dose-dependent manner in HEK293/IL-1RI

99   cells. K(D)PT was most effective at 5 μmol; 2.5 μmol K(D)PT had a notable effect,

100   while 1.25 μmol K(D)PT had little effect.
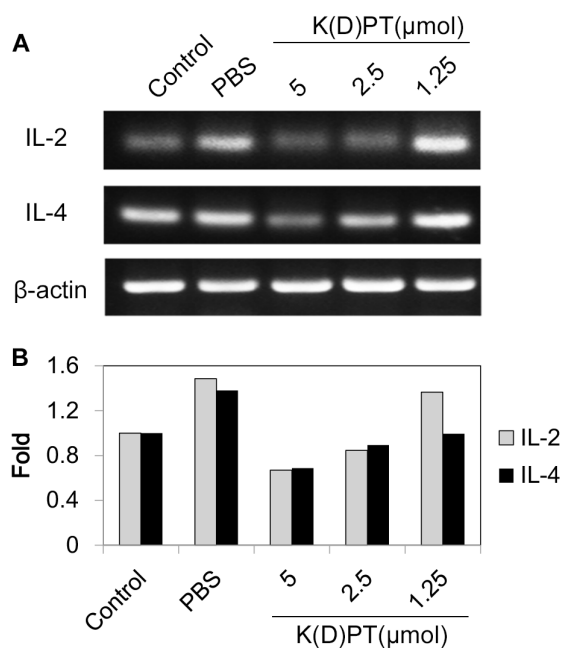
101

102   Figure 1. K(D)PT down-regulated the IL-1β-induced mRNA expression of the

103   downstream cytokines IL-2 and IL-4. The cells were treated with K(D)PT at various

104   concentrations for 2 hours and then stimulated with IL-1β for an additional 2 hours. In

105   the control group, both K(D)PT and IL-1β were replaced with PBS. In the PBS group,

106   K(D)PT was replaced with PBS. A: mRNA expression of IL-2 and IL-4. B:

107   IL-2/β-actin and IL-4/β-actin.

108

109   2.2 K(D)PT alleviates nasal symptoms of mice with allergic rhinitis

110   Nose itching, a major symptom of allergic rhinitis[35], results in nose scratching

111   and causes much discomfort, greatly affecting the quality of life of patients with

112   allergic rhinitis[36]. To obtain a mouse model of allergic rhinitis, C57BL/6 mice were

113   sensitized to OVA via intraperitoneal OVA injection and then challenged with an

114   intra-nasal dose of OVA. After each treatment, the frequency of nasal scratching was

115   observed for 5 minutes (Figure 2). Compared with saline-treated mice, the

116   OVA-treated mice exhibited a significant increase in nasal scratching. K(D)PT

117   treatment at different doses significantly decreased nasal scratching, whereas saline

118   had no effect. In addition, the efficacy of K(D)PT was comparable to that of cetirizine,

119   the second generation antihistamine widely used for treating AR[37, 38]. The effects of

120   K(D)PT were not substantially affected by different doses and this is in agreement

121   with previous reports for this compound[29]. This behavior may mean that the

122   interaction of K(D)PT and IL-1RI *in vitro* is isolated, but the interaction can be

123   influenced by many other cytokines *in vivo*.
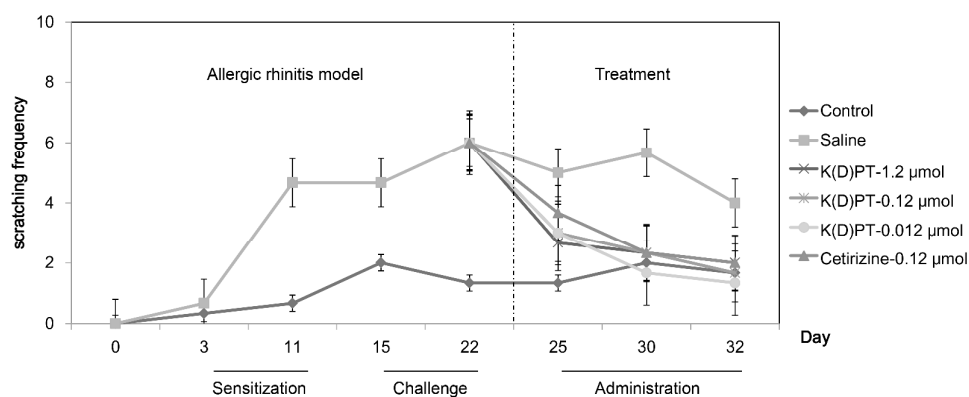
124

125

126   Figure 2. K(D)PT prevents the development of nasal scratching. Control: healthy mice

127   treated with an equivalent volume of saline throughout the experiment. Saline: mice

128   with allergic rhinitis treated with saline during the treatment period. The experimental

129   mice were treated with different doses of K(D)PT or cetirizine (n = 5). The data are

130   presented as the mean ± SE.

131

132   2.3 K(D)PT prevents the infiltration of nasal eosinophilia

133   People with allergic rhinitis experience histological changes in their nasal

134   mucosa, such as varying degrees of inflammatory cell infiltration, solid edema, and

135   epithelial damage. In this study, we assessed the distribution and severity of

136   allergen-induced sub-mucosal eosinophilic infiltration. H&E staining indicated that

137   the membrane of nasal mucosa tissue was intact in the control group (Figure 3). In the

138   mice that were sensitized to OVA, we observed cilia loss and solid edema. In addition,

139   mucosal eosinophil infiltration (bright red staining) was significantly greater in the

140   OVA-sensitized mice than in the control mice. After cetirizine treatment, eosinophil

141   infiltration was significantly alleviated, solid edema was slightly relieved, and cilia

142   loss was recovered. Treatment with 0.12 or 1.2 μmol of K(D)PT improved the

143   morphology of the mucosa tissue by relieving solid edema and decreasing eosinophil

144   infiltration; the low dose of 0.012 μmol of K(D)PT was not sufficient because allergic

145   inflammatory cell infiltration remained, although solid edema was relieved.
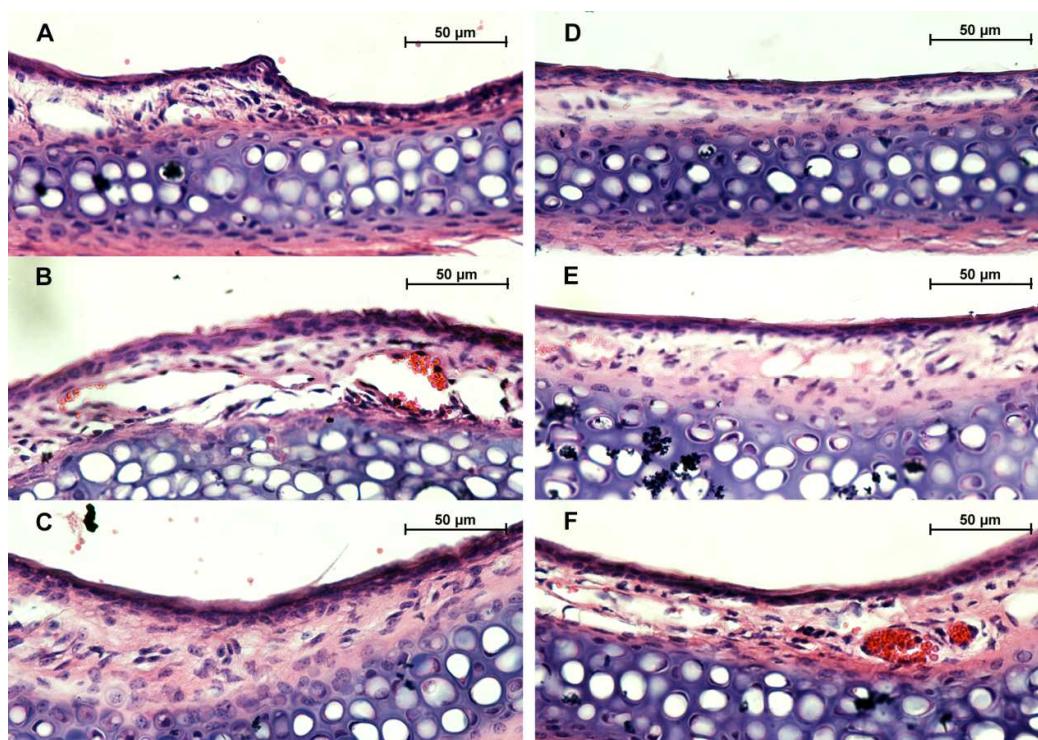
146
147   Figure 3. Nasal mucosa stained with H&E. Images were obtained using a 400× lens.

148   A: Control: healthy mice. B: Negative control: allergic rhinitis model. Mice with

149   allergic rhinitis treated with saline. C: Cetirizine group: mice with allergic rhinitis

150   treated with 0.12 μmol of cetirizine as a positive control. D, E, and F: Mice with

151   allergic rhinitis treated with 1.2, 0.12, or 0.012 μmol of K(D)PT.

152

153   2.4 K(D)PT down-regulates inflammatory cytokines in mouse serum

154   Considering the importance of IL-2 and IL-4 in T cell-mediated inflammation[34],

155   we determined the levels of IL-2 and IL-4 in mouse serum. Serum IL-2 and IL-4

156   levels were significantly up-regulated in sera from OVA-sensitized mice compared

157   with normal mice (Figure 4). After treatment with cetirizine or different doses of

158   K(D)PT, IL-2 and IL-4 levels were notably lower, suggesting that K(D)PT inhibits

159   inflammation. These data indicate that IL-1RI is involved in inflammatory diseases.
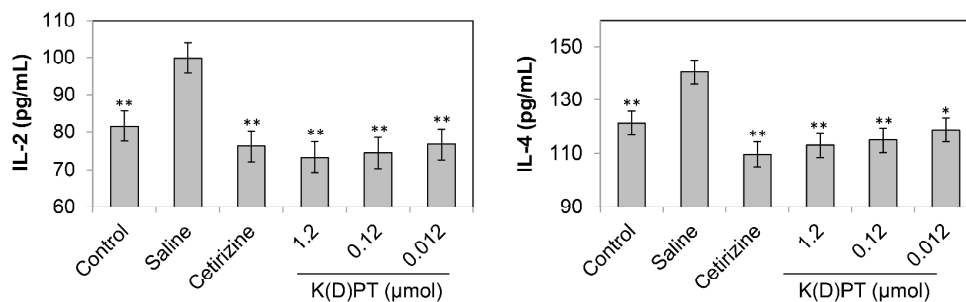
160

161   Figure 4. K(D)PT down-regulates inflammatory cytokines in mouse serum. Control:

162   healthy mice. Saline (negative control): mice with allergic rhinitis were treated with

163   saline during the treatment period after sensitization. Experimental: mice with allergic

164   rhinitis were treated with different doses of K(D)PT or 0.12 μmol of cetirizine. The

165   data are presented as the mean ± SE. Compared with the Saline group: * P < 0.05; **

166   P < 0.005; (n = 5).

167

168   2.5 IL-1RI is highly expressed in animals with allergic rhinitis

169   Immunohistochemistry was performed to verify IL-1RI expression in the nasal

170   mucosa of mice after various treatments. K(D)PT decreased IL-1RI expression

171   (Figure 5). IL-1RI was highly expressed in mice with allergic rhinitis (Figure 5B),

172   indicating that IL-1RI is a target for the treatment of inflammatory disease. After

173   treatment with 0.12 μmol of K(D)PT or cetirizine daily, IL-1RI expression was

174   significantly reduced in the mice. In summary, K(D)PT exerts anti-inflammatory

175   activity by reducing the expression of IL-1RI under inflammatory conditions.
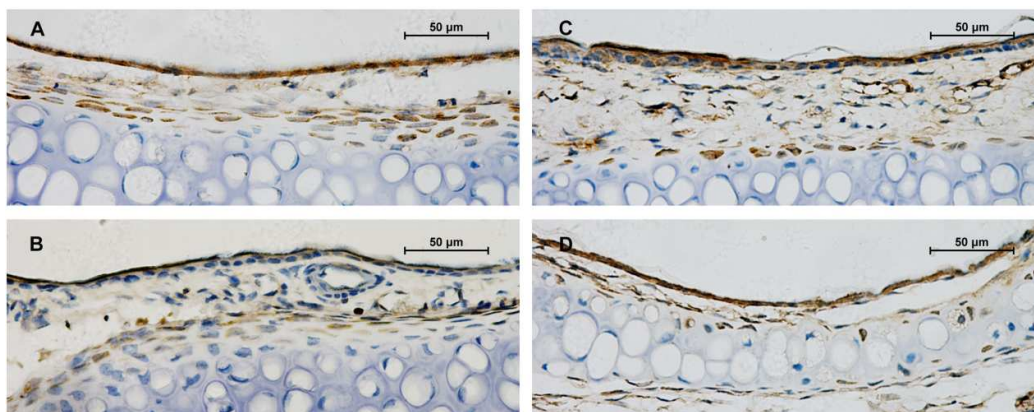
176

177   Figure 5. K(D)PT reduces IL-1RI expression. IL-1RI is indicated by blue staining in

178   nasal mucosa sections from mice. The images were obtained using a 400× lens. A:

179   Blank control: nasal mucosa from healthy mice. B: Negative control: nasal mucosa

180   from mice with allergic rhinitis treated with saline. C: K(D)PT group: nasal mucosa

181   from mice with allergic rhinitis treated with 0.12 μmol of K(D)PT. D: Positive control:

182   nasal mucosa from mice with allergic rhinitis treated with 0.12 μmol of cetirizine.

183

184   2.6 Molecular mechanism of action of K(D)PT as an IL-1RI antagonist

185   Fifty-ns MD simulations on the three systems (unliganded IL-1RI, the

186   IL-1RI/IL-1β complex, and the IL-1RI/K(D)PT complex) indicated that the backbone

187   RMSD of IL-1RI in the IL-1RI/IL-1β complex did not undergo notable fluctuations

188   during the entire simulation (Figure 6A). This result is consistent with the snapshots

189   extracted from the MD trajectories. The conformations of the IL-1RI/IL-1β complex

190   did not undergo major changes (Figure 6B), and the structure remained open.

191   The top-ten docked poses of K(D)PT were chosen as starting points for MD

192   simulations. Ten ns MD simulations demonstrated that one of the ten poses represents

193   stable conformation. Therefore, this pose was used as the starting point to conduct

194   MD simulations. Fifty-ns MD simulation indicated: the backbone RMSD of IL-1RI in

195   the IL-1RI/K(D)PT complex underwent significant change at approximately 3 ns and

196   remained relatively stable after 3 ns. The structure of the IL-1RI/K(D)PT complex

197   remained closed (Figure 6A) during the entire simulation. Initially, IL-1RI formed a

198   pocket (residues 240-264) to host K(D)PT. Hydrogen bonds formed between K(D)PT

199   (Lys and Thr) and IL-1RI (Glu253, Ile244 and Trp237). During the first 5 ns of the

200   simulation, the IL-1RI conformation changed from open to closed (Figure 6B) and

201   remained closed since then. This closed conformation is consistent with the crystal

202   structure (PDB code: 1G0Y) reported by Vigers[31]. Meanwhile, the K(D)PT

203   conformation underwent minor adjustments to accommodate the groove at the

204   C-terminal of IL-1RI (Figure 7). Between 5 and 25 ns in the simulation, the K(D)PT

205   conformation significantly changed; the hydrogen bonds between K(D)PT and IL-1RI

206   (at Trp237 and Asp245) were destroyed, and the Lys residue in K(D)PT flipped to

207   form new hydrogen bonds between K(D)PT (at Lys) and IL-1RI (at Ile244, Glu246,

208   and Glu253) at the C-terminal (Figure 7). Meanwhile, hydrogen bonds formed

209   between the Thr in K(D)PT and Glu2 (at the N-terminal) of IL-1RI (Figure 7).

210   The backbone RMSD of unliganded IL-1RI underwent large fluctuations during

211   the entire simulation (blue curve in Figure 6A). In the absence of ligand, IL-1RI was

212   flexible and capable of recruiting a ligand. The conformation of unliganded IL-1RI

213   randomly switched between open and closed (Figure 6B).

214   Principal component analyses (PCA) of the MD trajectories of the

215   IL-1RI/K(D)PT complex and unliganded IL-1RI identified the most significant

216   motions of the IL-1RI/K(D)PT complex and unliganded IL-1RI. The first two

217   principal components of the IL-1RI/K(D)PT complex accounted for 60.1% and 24.4%

218   of the overall motion; the first two principal components of unliganded IL-1RI

219   accounted for 46.7% and 4.2% of the overall motion. For the IL-1RI/K(D)PT complex,

220   the first component (PCA1) consisted of mainly the closing motion (Figure 8A):

221   domains I and III moved closer to each other. The second component (PCA2)

222   contained several motions (Figure 8B): domains I and III twisted counter-clockwise

223   toward the same plane. To summarize, K(D)PT induced IL-1RI to adopt a closed state

224   by forming hydrogen bonds with domains I and III.

225   In the unliganded IL-1RI system, domains I and III were connected to domain II

226   and randomly moved closer or apart (Figures 8C and 8D).

227   Energy landscape maps for the three systems, IL-1RI/K(D)PT (Figure 9A),

228   unliganded IL-1RI (Figure 9B), and IL-1RI/IL-1β (Figure 9C), were generated from

229   the 50 ns MD simulations. The energy landscape map of the IL-1RI/K(D)PT complex

230   revealed declining system energy path, starting with a sharp energy decrease of

231   approximately -5 kcal/mol at -25 of PCA1 (equivalent to approximately 25 ns) to

232   approximately -8 kcal/mol at 50 of PCA1 (equivalent to approximately 50 ns) (Figure

233   9A).

234   However, the energy landscape map of unliganded IL-1RI indicated that the

235   system energy remained nearly the same, approximately -6 kcal/mol, during the entire

236   simulation. The system energy evolution path was random (Figure 9B). The

237   IL-1RI/IL-1β system exhibited similar behavior (Figure 9C).

238   The energy landscape analyses further demonstrated that K(D)PT stabilizes the

239   closed conformation of IL-1RI.

240
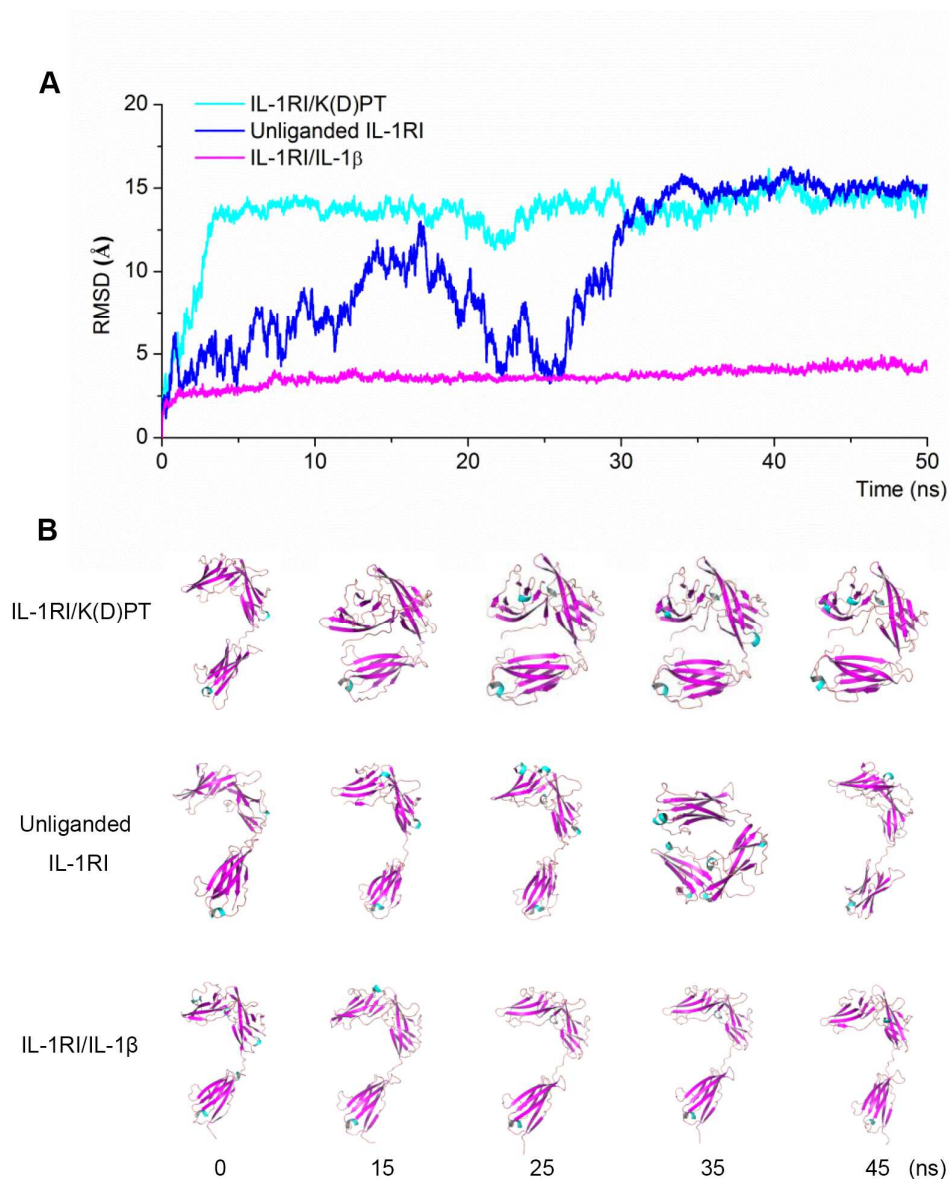
Figure 6. Backbone RMSD curves and conformational snapshots. A: Backbone
RMSD curves of the IL-1RI/K(D)PT, unliganded IL-1RI, and IL-1RI/IL-1β systems
generated from the 50 ns MD simulations. B: Snapshots taken from the MD
trajectories at different simulation time points to illustrate the conformational changes
of the systems. All three simulations were reproduced in differed heating or
equilibration protocol.

247
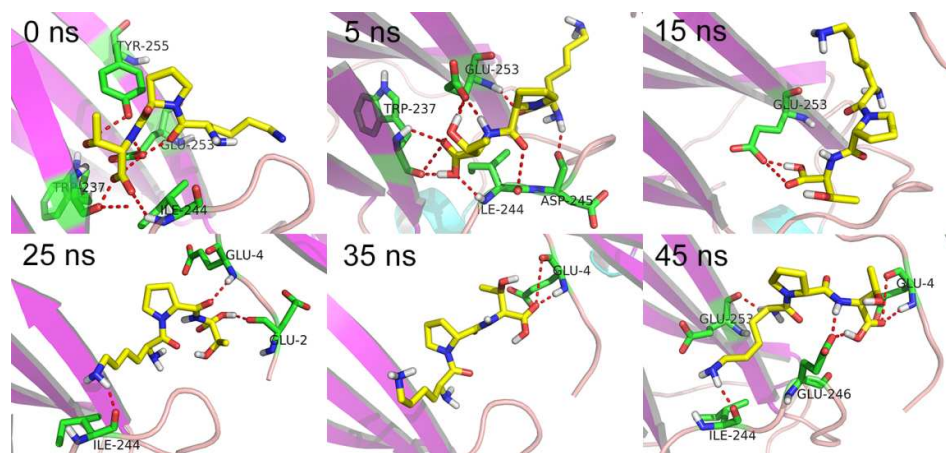
Figure 7. Initially, K(D)PT interacts only with C-terminal. After 50 ns MD simulations, K(D)PT interacts with both C- and N- terminals of IL-1RI via hydrogen bonds. K(D)PT, the active residues, and the backbone are colored in yellow, green, and pink, respectively.
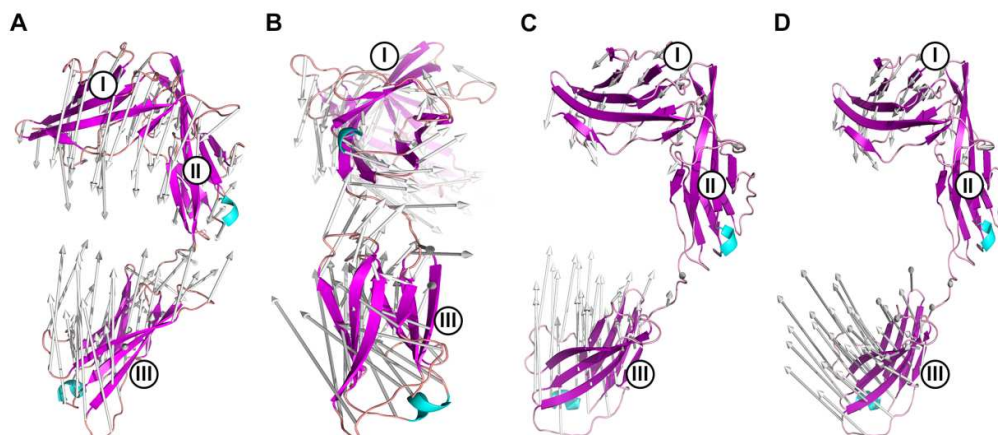
Figure 8. Principal component analyses (PCA) of the MD trajectories of the IL-1RI/K(D)PT complex and unliganded IL-1RI. A: PCA1 of the IL-1RI/K(D)PT complex. B: PCA2 of the IL-1RI/K(D)PT complex. C: PCA1 of unliganded IL-1RI. D: PCA2 of unliganded IL-1RI.
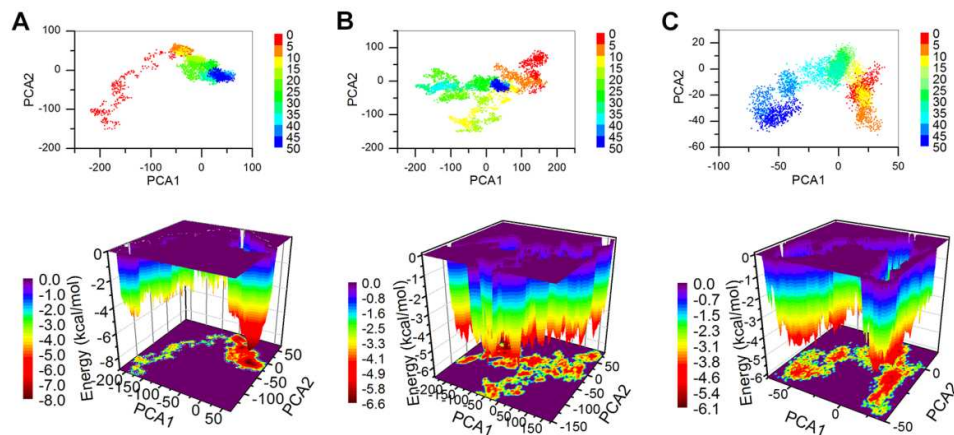
260

261 Figure 9. Energy landscape maps for the IL-1RI/K(D)PT, unliganded IL-1RI, and

262 IL-1RI/IL-1β systems generated from the 50 ns MD simulations. The top panel

263 contains projections of the snapshots onto PCA1 and PCA2, showing the motion trail

264 of the systems. The bottom panel includes the 3D free-energy landscapes, indicating

265 the temporal change in free energy. A: IL-1RI/K(D)PT complex. B: unliganded

266 IL-1RI. C: IL-1RI/IL-1β complex.

267

268 **3.   Experimental**

269 3.1 Ethics statement

270   This study was performed in strict accordance with the recommendations of the

271 Institutional Animal Care and Use Committee of Sun Yat-Sen University (IACUC,

272 SYSU). All procedures were approved by the Animal Ethical and Welfare Committee

273 of Sun Yat-Sen University. All efforts were made to minimize suffering.

274

275 3.2 Cell culture and stimulation

276   HEK293/IL-1RI cells stably expressing IL-1RI[15] were a kind gift from Dr. X. Li

277 (Cleveland Clinic, OH, USA). The cells were cultured in Dulbecco's modified Eagle's

278 medium (DMEM) supplemented with 10% fetal bovine serum (FBS), 100 U/ml

279 penicillin and 100 μg/ml streptomycin at 37°C in 5% CO_2. For stimulation, the cells

280 were seeded into 6-well micro-plates. At 80% confluence, the cells were treated with

281 K(D)PT (Jetway, Guangzhou, China) at the indicated concentrations for 2 hours.

282 IL-1β (1 ng/ml) was then added, and the cells were incubated for an additional 2 hours.

283   The cells were then harvested for further analysis.

284

285   3.3 Reverse-transcription PCR

286   Total RNA was isolated using RNAiso Plus (TaKaRa, Dalian, China) according

287   to the manufacturer's protocol. Total RNA (1 μg) was converted to cDNA using Oligo

288   (dT) 18. cDNA was used to amplify specific target genes by PCR. β-actin was used as

289   the RNA loading control. The PCR products were separated on 1% (w/v) agarose gels

290   and analyzed using an Alpha Imager EP (Alpha Innotech Corp., CA, USA). The

291   following   PCR   primer   sequences   were   used: β-actin,   sense

292   5'-TGGAATCCTGTGGCATCCATGAAA-3'   and   antisense

293   5'-TAAAACGCAGCTCAGTAACAGTCC-3';   IL-2,   sense   5'-

294   TCCAGAACATGCCGCAGAG-3'   and   antisense   5'-

295   CCTGAGCAGGATGGAGAATTACA-3';   and   IL-4,   sense   5'-

296   TCGACACCTATTAATGGGTCTCACC-3'   and   antisense   5'-

297   CAAAGTTTTGATGATCTCCTGTAAG-3'.

298

299   3.4 Animal study

300   Male 4- to 6-week-old C57BL/6 mice were purchased from the Medical

301   Experimental Animal Center of Guangdong province. All animals were housed under

302   Specific Pathogen Free (SPF) conditions at the Laboratory Animal Center of Sun

303   Yat-Sen University. All animal experiments in this study were approved by the

304   Animal Ethical and Welfare Committee of Sun Yat-Sen University.

305   The allergic rhinitis model was developed according to the method published by

306   Hiroko Saito[39] with a few modifications. Briefly, after 3 days of adaptive feeding, the

307   mice were sensitized with an intraperitoneal injection of 10 μg of ovalbumin (OVA,

308   Sigma, St. Louis, USA) in combination with 2 mg of aluminum hydroxide (ALU,

309   Shanghai Chemical Reagent Factory, Shanghai, China) dissolved in saline every

310   second day for a total of 7 injections as a general immunization. The mice in the

311   normal control group were given an intraperitoneal injection of saline on the same

312   schedule. After the general immunization, the mice received daily intra-nasal

313   challenges with 4 µl of a 10% OVA solution in saline (g/ml) for 10 days (600

314   µg/day), while the mice in the normal control group received intra-nasal challenges

315   with saline.

316   As a treatment, the sensitized mice received an intra-nasal dose of cetirizine or

317   K(D)PT at different dosages once a day for 10 days. For the control and negative

318   control, an equivalent amount of saline was administered in the same manner.

319

320   3.5 Nasal symptoms

321   To count the number of nasal scratching incidents, all mice were observed for 5

322   minutes after challenge in accordance with the method published by Masanori M.[40].

323

324   3.6 Cytokine assays

325   Twenty-four hours after the last nasal challenge, blood specimens were collected

326   from the mouse orbit and centrifuged at 2000 rpm for 20 minutes; serum was

327   collected and stored at -70°C. To measure the concentrations of IL-2 and IL-4 in the

328   mouse serum, commercially available ELISA kits (Dakewe Biotech, Beijing, China)

329   were used in accordance with the manufacturer's instructions. Each sample was

330   measured in triplicate.

331

332   3.7 Histological examination

333   To evaluate the infiltration of inflammatory cells into the nasal mucosa,

334   histological examinations were performed according to the method published by

335   Mitsuhiro Okano[41]. Briefly, the mice were sacrificed after blood collection, and their

336   heads were removed and fixed in a 10% neutral-buffered formalin solution for two

337   weeks, followed by removal of the nasal mucosa and embedding in paraffin. We then

338   followed the standard procedure for processing biopsy samples with H&E

339   (hematoxylin and eosin) staining. For immunohistochemistry, the samples were

340   deparaffinized and prepared according to standard protocols. IL-1RI was labeled with

341   an IL-1RI antibody (M-20, Santa Cruz, USA) and then detected using a ChemMate[TM]

342   DAKO Envision[TM] Detection Kit (DAKO, Glostrup, Tokyo, Denmark) with

343 diaminobenzidine staining. Images were acquired on a microscope (Nikon Eclipse 55i,

344 Japan) equipped with a CCD digital camera (Nikon DS-U3, Tokyo, Japan) and

345 analyzed with dedicated Firmware DS-U2 (Nikon, Tokyo, Japan). Constant condenser

346 and light intensity settings were used throughout the imaging process.

347

348 3.8 Statistical analysis

349   The data were analyzed by the unpaired *t*-test using the SPSS software and are

350 presented as the mean ± SE. P values of less than 0.05 were considered statistically

351 significant.

352

353 3.9 Molecular dynamics simulations

354   The extracellular structure of IL-1RI was obtained from the crystal structure

355 (PDB code: 4DEP)[23]. Missing residues (residues 34-35, 44-47, and 224-225 in the

356 loops of IL-1RI; residues 227-242, 268-275, and 297-309 in the loops of IL-1RAcp)

357 were fixed using the homology modeling module of Molecular Operating

358 Environment 2012.10 (MOE, Chemical Computing Group Inc. Montreal, Canada). To

359 study the impact of K(D)PT on IL-1RI, three systems were constructed. In the first

360 system, K(D)PT was docked into the loop between two β strands (fragment 240-264)

361 located in the third Ig-like domain of IL-1RI using the dock module of MOE[42]. The

362 ligand coordinates were taken from docking result. The structure of K(D)PT was

363 subjected to geometric optimization using the HF/6-31G(d) basis set from Gaussian

364 09[43]. The second system consisted of IL-1RI only, and the third system contained

365 IL-1RI and its endogenous ligand, IL-1β.

366   GPU-based[44, 45] MD simulations were performed using the PMEMD module in

367 AMBER 12[46]. The partial atomic charges of the ligands were calculated in the

368 Gaussian 09[43] program using the Hartree-Fock method with the 6-31G(d) basis set.

369 The antechamber program was then used to fit the restricted electrostatic potential

370 (RESP) and to assign the GAFF force field parameters[47]. For the proteins, the

371 AMBER ff12SB force field was used[48, 49]. The ligand-receptor complexes were

372 neutralized by adding sodium/chlorine counter ions and were solvated in an

373   octahedral box of TIP3P[50] water molecules with solvent layers of 10 Å between the

374   box edges and the solute surface. The SHAKE[51, 52] algorithm was used to restrict all

375   covalent bonds involving hydrogen atoms with a time step of 2 femtoseconds (fs).

376   The Particle-mesh Ewald (PME) method[53] was applied to treat long-range

377   electrostatic interactions.

378   For each ligand-receptor system, three steps of minimization were performed

379   before the heating step. First, all atoms in the receptor-ligand complex were restrained

380   with 50 kcal/(mol•Å^2), whereas the solvent molecules were not restrained. This step

381   included 2,000 cycles of steepest descent minimization and 2,000 cycles of

382   conjugated gradient minimization. Second, all heavy atoms were restrained with 10

383   kcal/(mol•Å^2) during the minimization steps, which included 2,500 cycles of steepest

384   descent minimization and 2,500 cycles of conjugated gradient minimization. The third

385   step included 5,000 cycles of steepest descent minimization and 5,000 cycles of

386   conjugated gradient minimization without restraint.

387   After the energy minimizations, the whole system was first heated from 0 to 300

388   K in 50 picoseconds (ps) using Langevin dynamics at a constant volume and then

389   equilibrated for 400 ps at a constant pressure of 1 atm. A weak constraint of 10 kcal/

390   (mol•Å^2) was used to restrain all heavy atoms in the receptor-ligand complexes during

391   the heating steps. Finally, periodic boundary dynamic simulations were conducted on

392   the whole system with an NPT (constant composition, pressure, and temperature)

393   ensemble at a constant pressure of 1 atm and 300 K in the production step. Each

394   receptor-ligand solution complex was simulated for 50 ns. The coordinates of each

395   system were saved every 10 ps. The root-mean-square deviations (RMSDs) of the

396   original receptors in the complexes were calculated.

397

398   3.10   Principle component analysis

399   Principle component analysis (PCA)[54] was utilized to ascertain the collective

400   motions of each system using the positional covariance matrix C of the atomic

401   coordinates and its eigenvectors. The elements of the positional covariance matrix C

402   were defined by Eq. (1):

403 $$C_i = \langle(x_i - \langle x_i \rangle)(x_j - \langle x_j \rangle)\rangle \ (i, j = 1, 2, 3, ..., 3N) \qquad (1),$$

404 where x_i is the Cartesian coordinate of the ith C_α atom, N is the number of C_α atoms

405 being evaluated, and $\langle x_i \rangle$ represents the time average over all configurations obtained

406 in the simulation. The eigenvectors of the covariance matrix, V_k, obtained by solving

407 $V_k^T C V_k = \lambda_k$ represent a set of 3N-dimensional directions or principal modes along

408 which the fluctuations observed in the simulation are uncoupled with respect to each

409 other and can be analyzed separately.

410

411 3.11   Energy landscape analysis

412   The energy landscapes of the proteins during the conformational changes were

413 obtained using an appropriate conformational sampling method. Conformations

414 produced by the MD simulations were used for the energy analysis in this study. A

415 covariance matrix of C_α was generated and used to analyze 3 eigenvectors to obtain

416 modes for each eigenvector. After calculating the 3 eigenvectors, snapshots were then

417 projected onto these eigenvectors in an additional sweep through the trajectory. In a

418 scatter diagram based on the two eigenvectors, the energy decreased as the intensity

419 of the projections increased. Thus, to obtain a three-dimensional (3D) representation

420 of the energy landscape, we divided the "scatter diagram" into N*N gridding and

421 calculated the distribution probability of each grid. The energy landscape was then

422 obtained using Eq. (2):[55-57]

423 $$G(x) = -k_B T * \ln P(x) \qquad (2),$$

424 where k_B is the Boltzmann constant, T is the temperature of the simulation, and P(x) is

425 the distribution probability. The energy surface was further smoothed using a

426 Gaussian kernel function, and the graphic views were generated using Origin 8.

427

428 **4. Conclusion**

429   Using HEK293/IL-1RI cellular assays and animal models, we determined that

430 IL-1RI antagonist K(D)PT exhibits anti-rhinitis activity. At the cellular level, K(D)PT

431 down-regulated the IL-1β-mediated induction of IL-2 and IL-4 mRNA expression. In

432 a mouse model, K(D)PT suppressed the inflammation-induced increase in serum IL-2

433 and IL-4. In addition, K(D)PT alleviated nose itching, mucosal eosinophil infiltration,

434 and solid edema in mice with allergic rhinitis.

435 Based on the 50 ns MD simulations, the following molecular mechanism of

436 action of K(D)PT as an IL-1RI antagonist can be proposed: (1) in the IL-1RI/IL-1β

437 complex, IL-1RI is in the open conformation; (2) in unliganded IL-1RI, domains I and

438 III randomly move closer or apart without significant energetic changes; (3) K(D)PT

439 induces IL-1RI to adopt a closed conformation by forming hydrogen bonds with

440 domains I and III. The closed conformation significantly reduces the system energy.

441 These findings provide novel avenues for the rational design of IL-1RI antagonists.

442

443 **5. Acknowledgements**

449

450 **6. Competing Interests**

451 The authors declare no competing financial interest.

452

453 **7. Author's Contributions**

454 The main concepts, experiment design, manuscript writing: CJL. Cell experiment:

455 CJL and YLL. Animal experiment: CJL, LJC, GDZ, YR and QH. Molecular dynamics

456 simulation and data analysis: CJL, HG, ZZZ, and BC. Revising and Submitting the

457 manuscript: QG and JX.

458

459

References

1. M. Benson, I. L. Strannegard, O. Strannegard and G. Wennergren, *The Journal of allergy and clinical immunology*, 2000, 106, 307-312.

2. Q. Hamid and M. Tulic, *Annual review of physiology*, 2009, 71, 489-507.

3. S. Romagnani, P. Parronchi, M. M. D'Elios, P. Romagnani, F. Annunziato, M. P. Piccinni, R. Manetti, S. Sampognaro, C. Mavilia, M. De Carli, E. Maggi and G. F. Del Prete, *International archives of allergy and immunology*, 1997, 113, 153-156.

4. D. Y. M. Leung, *Pediatr Res*, 1997, 42, 559-568.

5. F. M. Baroody and R. M. Naclerio, *Allergy*, 2000, 55, 17-27.

6. R. Uddman, L. Cantera, L. O. Cardell and L. Edvinnsson, *The Annals of otology, rhinology, and laryngology*, 1999, 108, 969-973.

7. M. Korsgren, J. S. Erjefalt, J. Hinterholzl, R. Fischer-Colbrie, C. A. Emanuelsson, M. Andersson, C. G. Persson, A. Mackay-Sim, F. Sundler and L. Greiff, *American journal of respiratory and critical care medicine*, 2003, 167, 1504-1508.

8. S. Dunzendorfer, P. Schratzberger, N. Reinisch, C. M. Kahler and C. J. Wiedermann, *Blood*, 1998, 91, 1527-1532.

9. A. J. Frew, *Journal of Allergy and Clinical Immunology*, 2003, 111, S712-S719.

10. H. S. Nelson, *Journal of Allergy and Clinical Immunology*, 2003, 111, S793-S798.

11. L. B. van de Putte, C. Atkins, M. Malaise, J. Sany, A. S. Russell, P. L. van Riel, L. Settas, J. W. Bijlsma, S. Todesco, M. Dougados, P. Nash, P. Emery, N. Walter, M. Kaul, S. Fischkoff and H. Kupper, *Annals of the rheumatic diseases*, 2004, 63, 508-516.

12. F. C. Breedveld, M. H. Weisman, A. F. Kavanaugh, S. B. Cohen, K. Pavelka, R. van Vollenhoven, J. Sharp, J. L. Perez and G. T. Spencer-Green, *Arthritis and rheumatism*, 2006, 54, 26-37.

13. S. T. Holgate and D. Broide, *Nature reviews. Drug discovery*, 2003, 2,

490   902-914.

491 14.   J. Sims, C. March, D. Cosman, M. Widmer, H. MacDonald, C. McMahan, C.

492   Grubin, J. Wignall, J. Jackson, S. Call and a. et, *Science*, 1988, 241, 585-589.

493 15.   Z. Cao, W. J. Henzel and X. Gao, *Science*, 1996, 271, 1128-1131.

494 16.   E. A. Kurt-Jones, S. Hamberg, J. Ohara, W. E. Paul and A. K. Abbas, *The*

495   *Journal of experimental medicine*, 1987, 166, 1774-1787.

496 17.   L. J. Rosenwasser, *The Journal of allergy and clinical immunology*, 1998, 102,

497   344-350.

498 18.   A. Courcoul, E. Vignot and R. Chapurlat, *Joint Bone Spine*, 2013, DOI:

499   10.1016/j.jbspin.2013.06.013.

500 19.   U. Huffmeier, M. Watzold, J. Mohr, M. P. Schon and R. Mossner, *The British*

501   *journal of dermatology*, 2013, DOI: 10.1111/bjd.12548.

502 20.   M. Braddock and A. Quinn, *Nature reviews. Drug discovery*, 2004, 3,

503   330-339.

504 21.   C. A. Dinarello, *Annual review of immunology*, 2009, 27, 519-550.

505 22.   L. A. O'Neill, *Immunological reviews*, 2008, 226, 10-18.

506 23.   C. Thomas, J. F. Bazan and K. C. Garcia, *Nature structural & molecular*

507   *biology*, 2012, 19, 455-457.

508 24.   T. Brzoska, T. A. Luger, C. Maaser, C. Abels and M. Bohm, *Endocrine reviews*,

509   2008, 29, 581-602.

510 25.   S. Grabbe, R. S. Bhardwaj, K. Mahnke, M. M. Simon, T. Schwarz and T. A.

511   Luger, *J Immunol*, 1996, 156, 473-478.

512 26.   T. E. Scholzen, *Endocrinology*, 2003, 144, 360-370.

513 27.   U. Raap, T. Brzoska, S. Sohl, G. Path, J. Emmel, U. Herz, A. Braun, T. Luger

514   and H. Renz, *J Immunol*, 2003, 171, 353-359.

515 28.   A. Kokot, A. Sindrilaru, M. Schiller, C. Sunderkotter, C. Kerkhoff, B. Eckes,

516   K. Scharffetter-Kochanek, T. A. Luger and M. Bohm, *Arthritis and*

517   *rheumatism*, 2009, 60, 592-603.

518 29.   A. Mastrofrancesco, A. Kokot, A. Eberle, N. C. J. Gibbons, K. U. Schallreuter,

519   E. Strozyk, M. Picardo, C. C. Zouboulis, T. A. Luger and M. Bohm, *The*

520   *Journal of Immunology*, 2010, 185, 1903-1911.

521   30.   D. Bettenworth, M. Buyse, M. Bohm, R. Mennigen, I. Czorniak, K.
522   Kannengiesser, T. Brzoska, T. A. Luger, T. Kucharzik, W. Domschke, C.
523   Maaser and A. Lugering, *The American journal of pathology*, 2011, 179,
524   1230-1242.

525   31.   G. P. Vigers, D. J. Dripps, C. K. Edwards, 3rd and B. J. Brandhuber, *The*
526   *Journal of biological chemistry*, 2000, 275, 36927-36933.

527   32.   D. S. Robinson, Q. Hamid, M. Jacobson, S. Ying, A. B. Kay and S. R. Durham,
528   *Springer seminars in immunopathology*, 1993, 15, 17-27.

529   33.   T. R. Mosmann and R. L. Coffman, *Annual review of immunology*, 1989, 7,
530   145-173.

531   34.   Q. Liang, L. Guo, S. Gogate, Z. Karim, A. Hanifi, D. Y. Leung, M. M. Gorska
532   and R. Alam, *J Immunol*, 2010, 185, 5704-5713.

533   35.   D. P. Skoner, *Journal of Allergy and Clinical Immunology*, 2001, 108, S2-S8.

534   36.   E. O. Meltzer, *Journal of Allergy and Clinical Immunology*, 2001, 108,
535   S45-S53.

536   37.   F. M. Baroody and R. M. Naclerio, *Allergy*, 2000, 55 Suppl 64, 17-27.

537   38.   P. J. Turner and A. S. Kemp, *Journal of paediatrics and child health*, 2012, 48,
538   302-310.

539   39.   H. Saito, K. Matsumoto, A. E. Denburg, L. Crawford, R. Ellis, M. D. Inman, R.
540   Sehmi, K. Takatsu, K. I. Matthaei and J. A. Denburg, *J Immunol*, 2002, 168,
541   3017-3023.

542   40.   M. Miyata, K. Hatsushika, T. Ando, N. Shimokawa, Y. Ohnuma, R. Katoh, H.
543   Suto, H. Ogawa, K. Masuyama and A. Nakao, *European journal of*
544   *immunology*, 2008, 38, 1487-1492.

545   41.   M. Okano, A. R. Satoskar, K. Nishizaki, M. Abe and D. A. Harn, Jr., *J*
546   *Immunol*, 1999, 163, 6712-6717.

547   42.   A. Mastrofrancesco, A. Kokot, A. Eberle, N. C. Gibbons, K. U. Schallreuter, E.
548   Strozyk, M. Picardo, C. C. Zouboulis, T. A. Luger and M. Bohm, *J Immunol*,
549   2010, 185, 1903-1911.

550　43.　M. J. Frisch, G. W. Trucks, H. B. Schlegel, G. E. Scuseria, M. A. Robb, J. R.

551　　　　Cheeseman, G. Scalmani, V. Barone, B. Mennucci, G. A. Petersson, H.

552　　　　Nakatsuji, M. Caricato, X. Li, H. P. Hratchian, A. F. Izmaylov, J. Bloino, G.

553　　　　Zheng, J. L. Sonnenberg, M. Hada, M. Ehara, K. Toyota, R. Fukuda, J.

554　　　　Hasegawa, M. Ishida, T. Nakajima, Y. Honda, O. Kitao, H. Nakai, T. Vreven, J.

555　　　　A. Montgomery, J. E. Peralta, F. Ogliaro, M. Bearpark, J. J. Heyd, E. Brothers,

556　　　　K. N. Kudin, V. N. Staroverov, R. Kobayashi, J. Normand, K. Raghavachari, A.

557　　　　Rendell, J. C. Burant, S. S. Iyengar, J. Tomasi, M. Cossi, N. Rega, J. M.

558　　　　Millam, M. Klene, J. E. Knox, J. B. Cross, V. Bakken, C. Adamo, J. Jaramillo,

559　　　　R. Gomperts, R. E. Stratmann, O. Yazyev, A. J. Austin, R. Cammi, C. Pomelli,

560　　　　J. W. Ochterski, R. L. Martin, K. Morokuma, V. G. Zakrzewski, G. A. Voth, P.

561　　　　Salvador, J. J. Dannenberg, S. Dapprich, A. D. Daniels, Farkas, J. B. Foresman,

562　　　　J. V. Ortiz, J. Cioslowski and D. J. Fox, Wallingford CT, 2009, DOI:

563　　　　citeulike-article-id:9096580.

564　44.　R. Salomon-Ferrer, A. W. Götz, D. Poole, S. Le Grand and R. C. Walker,

565　　　　*Journal of Chemical Theory and Computation*, 2013, DOI: 10.1021/ct400314y,

566　　　　130820111500003.

567　45.　A. W. Gotz, M. J. Williamson, D. Xu, D. Poole, S. Le Grand and R. C. Walker,

568　　　　*J Chem Theory Comput*, 2012, 8, 1542-1555.

569　46.　T. A. D. D.A. Case, T.E. Cheatham, III, C.L. Simmerling, J. Wang, R.E. Duke,

570　　　　R. Luo, R.C. Walker, W. Zhang, K.M. Merz, B. Roberts, S. Hayik, A. Roitberg,

571　　　　G. Seabra, J. Swails, A.W. Goetz, I. Kolossváry, K.F. Wong, F. Paesani, J.

572　　　　Vanicek, R.M. Wolf, J. Liu, X. Wu, S.R. Brozell, T. Steinbrecher, H. Gohlke,

573　　　　Q. Cai, X. Ye, J. Wang, M.-J. Hsieh, G. Cui, D.R. Roe, D.H. Mathews, M.G.

574　　　　Seetin, R. Salomon-Ferrer, C. Sagui, V. Babin, T. Luchko, S. Gusarov, A.

575　　　　Kovalenko, and P.A. Kollman, University of California, San Francisco, 2012.

576　47.　G. Mukherjee, N. Patra, P. Barua and B. Jayaram, *Journal of computational*

577　　　　*chemistry*, 2011, 32, 893-907.

578　48.　V. Hornak, R. Abel, A. Okur, B. Strockbine, A. Roitberg and C. Simmerling,

579　　　　*Proteins*, 2006, 65, 712-725.

580 49. W. D. Cornell, P. Cieplak, C. I. Bayly, I. R. Gould, K. M. Merz, D. M.
581   Ferguson, D. C. Spellmeyer, T. Fox, J. W. Caldwell and P. A. Kollman,
582   *Journal of the American Chemical Society*, 1995, 117, 5179-5197.

583 50. J. Wang, W. Wang, P. A. Kollman and D. A. Case, *Journal of Molecular*
584   *Graphics and Modelling*, 2006, 25, 247-260.

585 51. J.-P. Ryckaert, G. Ciccotti and H. J. C. Berendsen, *Journal of Computational*
586   *Physics*, 1977, 23, 327-341.

587 52. S. Miyamoto and P. A. Kollman, *Journal of computational chemistry*, 1992, 13,
588   952-962.

589 53. T. Darden, D. York and L. Pedersen, *The Journal of Chemical Physics*, 1993,
590   98, 10089.

591 54. A. Amadei, A. B. Linssen and H. J. Berendsen, *Proteins*, 1993, 17, 412-425.

592 55. E. Papaleo, P. Mereghetti, P. Fantucci, R. Grandori and L. De Gioia, *Journal of*
593   *molecular graphics & modelling*, 2009, 27, 889-899.

594 56. R. Zhou, B. J. Berne and R. Germain, *Proceedings of the National Academy of*
595   *Sciences of the United States of America*, 2001, 98, 14931-14936.

596 57. A. E. García and K. Y. Sanbonmatsu, *Proteins: Structure, Function, and*
597   *Bioinformatics*, 2001, 42, 345-354.

598

599